ELSEVIER

Water Research 38 (2004) 2726–2736

WATER RESEARCH

www.elsevier.com/locate/watres

Dynamics of lead immobilization in sulfate reducing biofilms

Haluk Beyenal[a], Zbigniew Lewandowski[a,b,*]

[a] *Center for Biofilm Engineering, Montana State University, P. O. 173980, Bozeman, MT 59717, USA*
[b] *Department of Civil Engineering, Montana State University, Bozeman, MT 59717, USA*

Received 13 March 2003; received in revised form 11 November 2003; accepted 18 March 2004

Abstract

We have evaluated the effects of selected minerals present in subsoil environment on the efficiency of lead removal from contaminated groundwaters using biofilms composed of sulfate-reducing microorganisms, and examined the stability of metal deposits after the biofilms had been temporarily exposed to the air. To quantify the studied effects, lead was immobilized in biofilms of *Desulfovibrio desulfuricans* grown anaerobically in two flat-plate flow reactors, one filled with hematite and the other with quartz. While the biofilms in both reactors were heterogeneous and consisted of voids and channels, the biofilms grown on hematite were denser, thicker, and more porous than those grown on quartz. The average H_2S concentrations, measured using microelectrodes, were higher in the biofilms grown on quartz than those measured in the biofilms grown on hematite. During 18 weeks of operation, iron was continuously released from the hematite. Lead was immobilized more efficiently in the biofilms grown on quartz than it was in the biofilms grown on hematite. Lead deposits were partially reoxidized, especially in biofilms grown on hematite, and the biofilms in both reactors responded to the presence of oxygen by lowering their density and increasing the H_2S production rate.
© 2004 Elsevier Ltd. All rights reserved.

Keywords: Sulfate-reducing bacteria; Lead; Iron; Biofilms; Biofilm heterogeneity; Biofilm structure; Biofilm activity

1. Introduction

Heavy metals in groundwaters can be immobilized by coprecipitating with hydrogen sulfide produced by sulfate-reducing bacteria (SRB) [1–4]. This process has potential for immobilizing contaminant heavy metals, such as Pb, Cu, Zn, Ni, Cd and U, in metal-contaminated groundwaters. However, before such a remediation process can be used with confidence, the stability of the metal deposits in the subsoil formation needs to be assessed. The two most obvious factors that may affect the stability of the metal deposits are: (1) the rate of H_2S production by the SRB biofilms and (2) the presence or ingress of oxidants. It is well known that the rate of H_2S production by SRB biofilms depends on the presence of the right population of microorganisms, nutrient availability, and a low redox potential [5]. If these conditions exist, it is expected that some heavy metals in solution will precipitate as their sulfides and that this process can be used to remediate groundwaters contaminated with these heavy metals. However, the overall metal removal efficiency may depend not only on the rate of H_2S production by SRB and the type of metal to be removed from the groundwater but also on the types of minerals present in the subsoil formation [6]. Specifically, if the minerals present in the subsoil formation release metal ions, other than ions of the metal to be removed, these released metal ions may compete with the contaminant metal ions for the metal-binding capacity of H_2S. This effect should be taken into consideration when attempting to remediate heavy-metal-contaminated groundwaters using SRB.

*Corresponding author. Tel.: +1-406-994-5915; fax: +1-406-994-6098.
E-mail address: zl@erc.montana.edu (Z. Lewandowski).

0043-1354/$ - see front matter © 2004 Elsevier Ltd. All rights reserved.
doi:10.1016/j.watres.2004.03.023

The goal of this study was to investigate the effects of selected minerals present in the subsoil environment on the efficiency of the target metal removal. To quantify how seriously this effect may impair the removal efficiency of the target metal, we grew sulfate reducing biofilms on quartz and on hematite, and used lead ions, Pb^{2+}, as the target metal. Lead ions were selected because lead sulfide, PbS, has one of the lowest solubility products among metal sulfides ($pK = 27.5$, [7]). Therefore, if the iron ions (Fe(II) or Fe(III)) released from the hematite could affect the rate of lead precipitation by exhausting the binding capacity of the microbially generated hydrogen sulfide, this effect should be magnified for other contaminating metals, those having higher solubility products than Pb has. For the purpose of this work, we hypothesized that the iron ions [Fe(II) or Fe(III)] released from the hematite react and precipitate with the microbially produced H_2S, thus indirectly affecting the dynamics of lead precipitation.

Quartz and hematite were selected to generate two types of microbe-mineral interactions: quartz, to represent biofilms growing on inert minerals that do not release metals competing with the target metal for the binding sites; and hematite, to represent biofilms growing on minerals that can release metals (iron in this case). It has been demonstrated by others, and was therefore expected, that the metals released from the minerals might use part of the overall metal binding capacity of the biofilms [6,8,9], affecting the removal efficiency of the target metal(s). While quantifying the effect of the selected minerals, the following assumptions were made with respect to the interfering processes. The effect of biosorption, the binding of lead ions by extracellular biopolymers was neglected because even if such binding contributed to the overall lead removal, the binding capacity of the biopolymers would be quickly exhausted, making this contribution negligible. It is also known that Fe(III) can be enzymatically reduced by SRB and remobilized as Fe(II) [6,10]. This effect, if at all active in our biofilms, was not quantified in our work. We also assume that the metals present in the solution are not toxic to the microorganisms, at least not at the concentrations we have used in our tests.

The chemical principles of lead removal using SRB biofilms are straightforward; SRB gain energy by coupling oxidation of organic compounds with the reduction of sulfate ions, and generate H_2S as the by-product [11]. Microbially generated H_2S dissolves in water and, being a diprotic acid, dissociates to bisulfide, HS^- and sulfides, S^{2-}:

$$H_2S \rightleftharpoons HS^- + H^+ \tag{1a}$$

$$HS^- \rightleftharpoons H^+ + S^{2-} \tag{1b}$$

In the presence of Pb^{2+} ions, bisulfide precipitates lead ions as lead sulfide, PbS, which can dissolve in the following reactions ((2a)—Ref. [12], (2b)—Ref. [7]):

$$PbS(s) + H^+ \rightleftharpoons HS^- + Pb^{2+} \quad pK = 13.97 \tag{2a}$$

$$PbS(s) \rightleftharpoons S^{2-} + Pb^{2+} \quad pK = 27.5 \tag{2b}$$

Assuming that there are no serious kinetic limitations, if Pb^{2+} ions were the only metal ions available, the process of lead precipitation would be simple to quantify. However, there are other metal ions in the solution, notably some released from the mineral phase serving as solid support for biofilm growth, such as iron ions from the hematite, and H_2S can precipitate Fe^{2+} in similar reactions ((3a)—Ref. [12], (3b)—Ref. [7]):

$$FeS(s) + H^+ \rightleftharpoons HS^- + Fe^{2+} \quad pK = 4.2 \tag{3a}$$

$$FeS(s) \rightleftharpoons S^{2-} + Fe^{2+} \quad pK = 18.1 \tag{3b}$$

The above data show that the solubility product of FeS is much higher than that of PbS, which in homogeneous aqueous solutions would indicate that Pb^{2+} ions have to precipitate before Fe^{2+} ions can precipitate. However, biofilms are not homogeneous solutions, and mass transport effects, and perhaps other reactions, such as chelation of the metal ions by organics or by the extracellular polymeric substances excreted by the biofilm microorganisms, may change the outcome of the process in an unexpected way. For that reason, in biofilms, conclusions based on the thermodynamics of metal ions in aqueous solutions alone are considered as working hypotheses, and tested as such, rather than accepted as axioms.

Once the target metal has been immobilized as the respective metal sulfide, another perturbing factor may have a negative effect on the efficiency of metal immobilization, the presence or ingress of oxidants. For example, it is expected that if oxygen becomes available, the precipitated metal sulfide deposits may be remobilized as metal hydroxides, oxides, and sulfates [8,13]. One possible reaction in our model is the effect of exposing lead sulfide to oxygen:

$$PbS(s) + 2O_2 \rightarrow PbSO_4(s) \tag{4}$$

However, the danger that $PbSO_4$ can dissolve and lead can be released to the bulk solution is probably negligible because lead sulfate does not dissolve easily:

$$PbSO_4(s) \rightleftharpoons Pb^{2+} + SO_4^{2-} \quad pK = 7.8 \tag{5}$$

Solubility product of $PbSO_4$ is very low, $K_{sp} = 10^{-7.8}$ [14]. Consequently, if the reaction of lead sulfides with oxygen produced lead sulfates, lead would not be released.

In addition, oxygen will react with hydrogen sulfide, therefore preventing lead sulfide formation:

$$H_2S + 2O_2 \rightleftharpoons H_2SO_4 \tag{6}$$

Fig. 1 summarizes the model we are considering as representative of the expected reactions in a biofilm

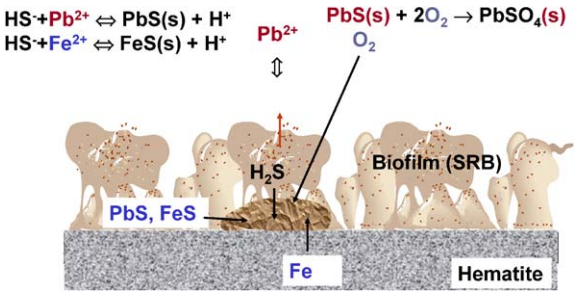

Fig. 1. Expected reactions among H_2S, lead and Fe in SRB biofilms grown on hematite. Note that these are simplified primary reactions.

composed of SRB growing on hematite. Even though the model is simplistic, and the processes we have shown in the model are straightforward, it is difficult to predict the dynamics of metal immobilization and remobilization in SRB biofilms grown in the subsoil environment; there are various interfering factors that may affect the outcome of these processes, and these factors are difficult to evaluate. Among the factors we consider most important are: (1) the effects of mass transport resistance in biofilms on metal availability, particularly in deeper layers of the biofilm, and (2) the dynamics of metal remobilization when oxidants are introduced into the milieu. In conclusion, comparing the solubility products of the depositing metals can serve only as a starting point for formulating hypotheses, not as a basis for modeling the stability of metal deposits in biofilms, particularly in biofilms deposited on redox-sensitive minerals.

To assess the efficiency of metal precipitation in natural biofilms, and the effects of the selected interfering factors, we studied biofilms of *Desulfovibrio desulfuricans* grown anaerobically on hematite and on quartz in two identical, and identically operated, flat-plate open channel flow reactors. Biofilm activity was defined as the H_2S production rate, and evaluated from the H_2S profiles measured using microelectrodes. Confocal scanning laser microscopy (CSLM) and image analysis were used to quantify biofilm structure. Concentrations of iron and lead were monitored in the bulk solution and in the biofilms. The possibility of metal remobilization through reoxidation of the precipitated deposits was evaluated by examining the stability of the metal deposits after the biofilms temporarily exposed to the air.

2. Experimental methods

2.1. Organisms

To grow the SRB biofilms we used a pure culture of *D. desulfuricans* (G20) developed from G100A and donated by J.D. Wall [15]. Fresh inoculums were prepared for each run by growing batch cultures of *D. desulfuricans* in 100-mL serum bottles for three days. The reactors were inoculated with 20 mL of these cultures.

2.2. Nutrient solution

To grow the biofilms, we used the "metal toxicity medium" (MTM) developed by Sani et al. [16], which minimized abiotic lead complexation and precipitation while still providing a suitable growth medium for *D. desulfuricans*. MTM is a Postgate medium C [17] modified by removing $FeSO_4$ and adding sodium lactate. MTM composition and the procedure of its preparation are described by Sani et al. [16].

The pH of the MTM solution was adjusted to 7.2 using 1 N HCl. 0.1 g ascorbic acid and 0.1 g sodium thioglycollate were added per liter of the growth medium to decrease the redox potential and to stimulate the growth of SRBs. However, these substances also acted as reductants and a small amount of lead precipitated after 24 h [16]. Therefore, they were removed from the growth medium after the biofilm started to accumulate (after approximately three days). Once a vigorous sulfate reducing biofilm was established, the redox potential was established at the desired low level by microbial metabolism, and the reductants were no longer needed [16,17]. In separate experiments, Sani et al. [16] showed that sodium citrate did not affect the growth of *D. desulfuricans* (G20) and that it could be used as a chelating agent to prevent metal precipitation. The concentration of yeast extract in the original Postgate C medium was decreased (20 times) because in the original medium unknown precipitates formed in the presence of Pb^{2+}, as described by Sani et al. [16]. The Pb^{2+} concentration in the feed solution was 30 mg/L.

2.3. The reactor

The biofilms were grown at room temperature on quartz and on hematite chips placed on the bottom of an open-channel flow reactor made of polycarbonate. The reactors were 3.5 cm deep, 2.5 cm wide, and 34 cm long, with a total working volume of 120 mL, as described elsewhere [18]. The quartz chips were $2.5 \times 7.5 \times 0.1\,cm^3$, and the hematite chips were $0.5 \times 0.5 \times 0.5\,cm^3$. The minerals were placed at the bottoms of the reactors, covering an area of $56.25\,cm^2$. Before deposition in the reactor, the hematite chips were cleaned with acetone, rinsed with distilled water, polished with sandpaper, and washed again with distilled water. The X-ray diffraction (XRD) data (results not shown) determined that the hematite chips were 90% hematite and 10% magnetite, and contained traces of cristobalite (Beta-SiO_2).

To prevent microbial contamination and air access, the lids of the reactors were sealed with silicon rubber and the reactors were sterilized with 70% alcohol before each experiment. The reactors were then rinsed with sterile water (autoclaved), for approximately three days using a total of 20–40 L of sterile water to remove alcohol residues. Tubings, connectors, air filters, and the growth medium were autoclaved at 121°C. During operation, the reactors were continuously purged with nitrogen gas to create positive pressure and to prevent air penetration into the system. To remove traces of oxygen from the nitrogen gas, the gas was passed through a tube furnace (Lindberg/Blue).

2.4. Analytical methods

The concentrations of lead and iron in the influent and effluent of the reactor were measured using induced coupled plasma (ICP) emission spectroscopy (ARL, model ♯ARL-Accuris). Liquid samples collected for metal analysis were centrifuged for 20 min at 6000 rpm. The pellet was discarded and the supernatant was analyzed. To determine the total lead and iron concentrations in the biofilms, the mineral chips with attached biofilm were removed from the reactor, and the biofilm was mechanically removed from the mineral surface. The biomass removed from the chips was suspended in distilled water, sonicated for 2 min, and then treated with 3 N nitric acid, HNO_3 to dissolve the precipitated metals [9]. Then the samples were centrifuged for 20 min at 6000 rpm, the pellet was discarded, and the supernatant was used for iron and lead analysis.

2.5. H_2S microelectrodes

The H_2S microelectrodes were constructed and used according to the procedure described by Jeroschewski et al. [19]. Their tip diameters were less than 10 μm to prevent damaging the biofilm structure during measurements. Operating principles of the H_2S microelectrodes are described in Beyenal and Lewandowski [18] and in Lewandowski and Beyenal [20]. The electrode was calibrated in water solutions with different H_2S concentrations, prepared by dissolving sodium sulfide, Na_2S, in oxygen-free 100-mM phosphate buffer at pH 7. The response time of the microelectrodes was less then 3 s and the response remained linear over a large H_2S concentration range, from 0 to 300 μM H_2S. Typically, the microelectrodes had the same calibration curves before and after the measurements, within the range of acceptable experimental error (±2 μM). We used a new microelectrode for each measurement.

2.6. Microelectrode measurements

To measure the H_2S concentration profiles in the biofilms, the microelectrodes were inserted into the reactor through a small opening in the lid while the system was continuously purged with nitrogen gas, creating a positive pressure in the reactor and preventing the ingress of air from the outside. The microelectrodes were mounted on a micromanipulator (Model M3301L, World Precision Instruments, New Haven, CT) equipped with a stepper motor (Model 18503, Oriel, Stratford, CT), and controlled by the Oriel Model 20010 interface. Microelectrodes were introduced from the top of the reactor, perpendicular to the biofilm. The position of the microelectrode within the biofilm was observed using an Olympus® CK2 inverted microscope (for biofilms grown on quartz) or a Leica® Stereo Zoom 7 stereo microscope (for biofilms grown on hematite). Different systems had to be used because the hematite chips were not transparent. The motorized micropositioner was interfaced with a computer, and the microelectrode movement was handled by a controller (CTC-283-3, Micro Kinetics) with 0.1-μm positioning precision. Custom software was used to control microelectrode movement and to coordinate it with the data acquisition (for more details, see [21]). The diffusive fluxes of H_2S into the bulk liquid were calculated by multiplying the slope of the profiles evaluated at the biofilm surface by the diffusion coefficient of H_2S in water ($D_{H_2S} = 1.7 \times 10^{-5}$ cm^2/s) [22].

2.7. Quantifying biofilm structure

To visualize biofilm structure hematite and quartz chips with attached biofilm were removed from the reactor and immersed in a separate vessel filled with 1%v/v acridine orange (from Sigma), as described by Xia et al. [23]. The mineral chips remained immersed, and the staining solution was recycled for 30 min to complete the staining before acquiring the images. The mineral chips were removed from the vessel, and the excess of the staining solution was removed by washing the mineral chips with the sterile growth medium. The mineral chips with the stained biofilm were placed on the stage of the upright confocal scanning laser microscope (LEICA, TCS NT). Biofilm images were collected at different distances from the bottom, and were used to quantify biofilm structure: biofilm porosity and fractal dimension, as described by Yang et al. [24]. These two parameters were selected from among many we measure in biofilms [24] because their meaning for biofilm processes is intuitively clear. Biofilm porosity affects the depth of substrate penetration (larger voids permit substrate transport to deeper layers of the biofilm), and biofilm fractal dimension is related to biofilm activity

(more rugged biofilms have larger surface areas per unit of volume).

2.7.1. Areal porosity

Areal porosity is defined as the ratio of the total areas of the interstitial voids to the total area of the biofilm image. It is quantified from individual images of the biofilm taken at various distances from the bottom. Numerically, biofilm areal porosity reflects the relative coverage of the surface by the biofilm: high porosity indicates low coverage, and low porosity indicates high coverage. As biofilms mature, their areal porosity decreases near the bottom, sometimes approaching a steady state [25]. A set of areal porosities determined at different distances from the bottom is used to quantify the volumetric porosity of the biofilm.

2.7.2. Volumetric porosity

Volumetric porosity was calculated using the procedure described in Lewandowski [26]. Briefly, to compute the volumetric porosity of the biofilms, areal porosities measured at different distances from the bottom of the biofilm were integrated, and the result of the integration was multiplied by the area of the image (field of view). The result of this procedure gives the volume of voids for the field of view. If we divide this result by the volume of the sample (field of view times average biofilm thickness) the result is the volumetric biofilm porosity, which is the ratio of the volume of the voids to the volume of the biofilm.

2.7.3. Fractal dimension

Fractal dimension is a measure of the "raggedness" of the microcolony boundaries: the higher the fractal dimension, the more irregular the boundaries. The fractal dimension of a biofilm can be, at least quantitatively, related to biofilm activity. The higher the fractal dimension, the more irregular the boundaries of biofilm microcolonies and the larger the surface area of the microcolonies exposed to the nutrient solution. However, although fractal dimension is used as a tool for quantifying biofilm structure, it does not characterize objects uniquely: two objects may have distinctly different geometries and still have the same fractal dimension [27]. Therefore, fractal dimension of biofilm microcolonies can be used as a measure of the convolution of boundaries of the microcolonies, rather than as a parameter uniquely quantifying biofilm structure. We expect that biofilms having more convoluted microcolony boundaries are more active than those with less convoluted boundaries, but this relation has not been quantified.

3. Results and discussion

3.1. Biofilm structure

3.1.1. Areal porosities and fractal dimensions

The biofilms in both reactors were heterogeneous, consisting of voids and cell clusters as shown in Fig. 2. To quantify the structure of each biofilm, we computed its areal porosity and fractal dimension at various distances from the bottom. The results are in Fig. 3 (for the 7-week-old biofilms) and Fig. 4 (for the 16-week-old biofilms).

Structure of the 7-week-old biofilms: The areal porosities measured across the biofilms grown on quartz were generally lower than those of the biofilms grown on hematite, showing that, on average, more biomass had accumulated in the biofilms grown on hematite. However, the distribution of the biomass near the bottom in

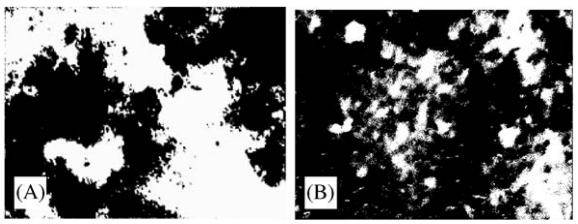

Fig. 2. Digitized confocal scanning laser microscopy images of the16-week-old biofilms grown on quartz (A) and hematite (B). The images were taken 200 μm above the substratum. The white areas are cell clusters, and the black areas are voids in the biofilms. The areal porosity of the biofilm grown on quartz was 0.63, and that of the biofilm grown on hematite was 0.77. The fractal dimension of the biofilm grown on quartz was 1.12 and that of the biofilm on hematite was 1.3.

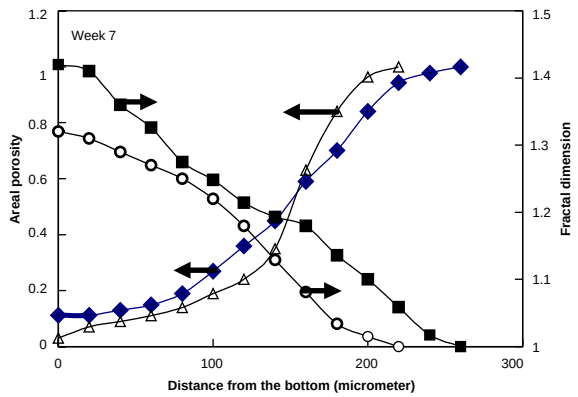

Fig. 3. The variation in areal porosity (A) and fractal dimension (B) in the 7-week-old biofilms. (The structure was analyzed before exposing the biofilms to the air.) Areal porosities; (♦) hematite and (△) quartz. Fractal dimensions; (■) hematite and (○) quartz.

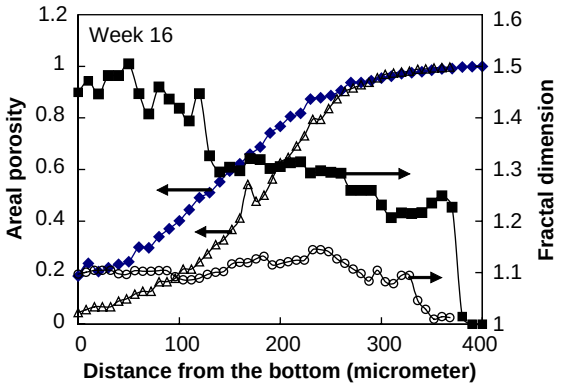

Fig. 4. The variation in biofilm areal porosity (A) and fractal dimension (B) in the16-week-old biofilms. (The structure was analyzed before exposing the biofilm to the air). Areal porosities; (♦) hematite and (△) quartz. Fractal dimensions; (■) hematite and (○) quartz.

these biofilms was reversed. The areal porosity near the bottom of the biofilm was 0.1 for biofilms grown on hematite, and zero for those grown on quartz. This shows that somewhat more biomass accumulated near the bottom in the biofilms grown on quartz. The differences in porosity near the bottom are not dramatic, just 10%, and it is not clear whether they are significant and meaningful to the biofilm processes.

Fractal dimensions at the bottom of the biofilm were: 1.42 in the biofilm grown on hematite and 1.3 in the biofilm grown on quartz, showing that the surface of the cell clusters in the biofilms grown on hematite was somewhat more developed than that of the cell clusters grown on quartz. Again, the differences are not dramatic, and it is not clear how significant they are for the biofilm processes.

Structure of the 16-week-old biofilms: The areal porosity measured near the bottom of the biofilms grown on hematite was 0.2, which is four times higher than that measured in the biofilms grown on quartz, 0.05. It is worth noting that this relation is the opposite of what was observed in the 7-week-old biofilms, which only reinforces our doubts about whether these variations are meaningful for the underlying biofilm processes. It is well known that the structure of mature biofilms is dynamic, affected by attachment and detachment processes, and that biofilm porosity may fluctuate because of the interplay between these processes. We do not know how different the porosities should be to be considered significantly different from the point of view of the underlying biofilm processes.

The fractal dimension near the bottom of the 16-week old biofilm was 1.45 for the biofilm grown on hematite and only 1.1 for the biofilm grown on quartz. We hypothesize that the higher fractal dimension of the biofilm grown on hematite was caused by the interaction between the biofilm and hematite: the iron ions dissolved from the hematite may have precipitated within the biofilm as iron sulfides, which may have affected the biofilm structure.

3.1.2. Volumetric porosities

From the results in Figs. 3 and 4 we calculated the volumetric porosities. The porosity of the 7-week-old biofilm grown on quartz was 0.33, and that of the one grown on hematite was 0.40. The porosity of the 16-week-old biofilm grown on quartz was 0.44, and that of the one grown on hematite was 0.59. Thus, the biofilms grown on hematite had consistently higher porosities than the biofilms grown on quartz. Since the only difference between the reactors were the minerals at which the biofilms accumulated, it is possible that iron ions released from hematite may have played a role in increasing volumetric porosities.

3.2. Biofilm activity

For the purpose of this study, biofilm activity was identified with the rate of H_2S production, which is equivalent to the flux of H_2S determined from the H_2S concentration profiles measured by microelectrodes. The H_2S concentration profiles that we used to determine biofilm activity are shown in Figs. 5A and B. The H_2S fluxes calculated from these profiles are in Table 1, and those from other measurements (results not shown) are in Fig. 6.

3.2.1. Comparing activities of biofilms grown on quartz with the activity of biofilms grown on hematite

The concentration of H_2S in biofilms grown on hematite was consistently lower than that in biofilms grown on quartz (Table 1, Fig. 5). This difference may have been related to the higher porosity of the biofilms grown on hematite compared to those grown on quartz (see Figs. 3 and 4), as more porous biofilms may have stimulate removal of hydrogen sulfide. However, it should be also noticed that the less porous biofilms had more biomass per unit of volume, which may have contributed to their higher activity.

It is worth noting that when both biofilms were exposed to atmospheric oxygen for the first time (weeks 8–10), the H_2S flux almost doubled. However, when the biofilms were exposed to oxygen for the second time (weeks 16–18), the H_2S flux remained almost constant, showing that at that time the biofilm activities were not affected by the presence of oxygen. This somewhat unexpected observation demonstrates that mature biofilms may respond differently to environmental challenges than young biofilms.

The H_2S fluxes calculated from Fig. 5 and other measurements are in Fig. 6. The H_2S flux was maximal

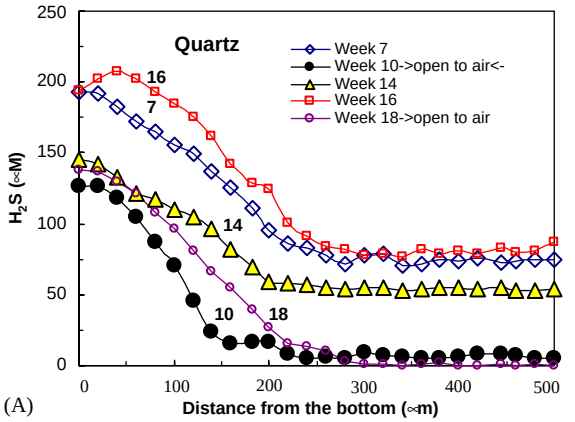

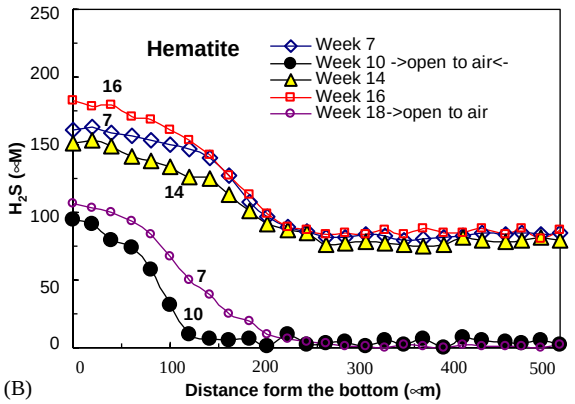

Fig. 5. H_2S profiles of the biofilms grown on quartz (A) and the biofilms grown on hematite (B). The data points marked as "open to air" were collected when the reactor was being continuously purged with filtered air for two weeks. Note that the numbers on the figures show the measurement time in weeks.

in both reactors when the biofilms were 10 weeks old. The subsequent decrease in the H_2S flux was likely caused by the changes in the internal biofilm structure, such as the decreased volumetric porosity (Figs. 3 and 4). The H_2S fluxes in both biofilms were stable between the 16th and 18th weeks. However, the H_2S flux was slightly higher (approximately 17%) in the biofilm grown on quartz than in that grown on hematite. This difference may have been caused by the fact that the H_2S concentration in the biofilm microcolonies growing on quartz was consistently higher that that in the biofilm microcolonies growing on hematite, as part of the H_2S generated in the biofilms growing on hematite was reacting with iron.

Biofilm thickness and density: The variation in biofilm density and thickness during biofilm growth, immobilization, and remobilization of lead deposits is shown in Figs. 7A and B. As time progressed, biofilm density in both biofilms gradually increased, reaching 90 g/L at the

Table 1
H_2S fluxes and concentrations calculated from the data in Fig. 5

Biofilm age (weeks)	Biofilm grown on quartz			Biofilm grown on hematite		
	The H_2S flux (μmole/cm^2/s)	H_2S concentration at the bottom of the biofilm (μM)	H_2S concentration in the bulk (μM)	The H_2S flux (μmole/cm^2/s)	H_2S concentration at the bottom of the biofilm (μM)	H_2S concentration in the bulk (μM)
1–6	Operated anaerobically					
7	9.3×10^{-5}	195	70	9.6×10^{-5}	161	80
8	The reactors exposed to air from the beginning of week 8 to the end of week 9. The measurements were performed at the beginning of the week 10.					
9						
10	16×10^{-5}	126	≈ 3–5	18.7×10^{-5}	94	≈0
11–13	Operated anaerobically					
14	8.3×10^{-5}	145	50	8.3×10^{-5}	151	75
15	Operated anaerobically. The measurements were performed at the beginning of week 16 right before exposing the biofilms to the air.					
16	12×10^{-5}	194	80	9.6×10^{-5}	182	85
17	The reactors exposed to air from the beginning of week 16 to the end of week 17. The measurements were performed at the beginning of the week 18.					
18	11.5×10^{-5}	137	≈0	9.4×10^{-5}	106	≈0

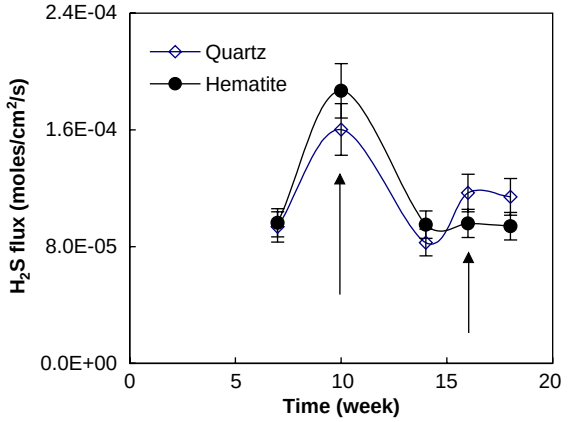

Fig. 6. H_2S fluxes calculated from Fig. 5 and other measurements. The arrows mark the times when the biofilms were exposed to the atmosphere.

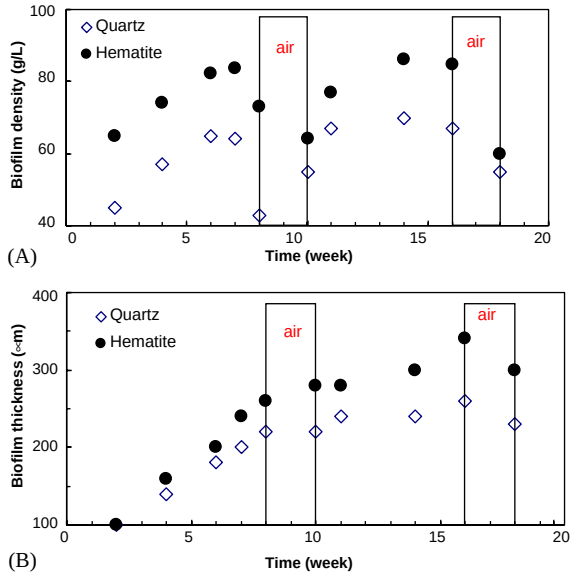

Fig. 7. Variation in biofilm density (A) and thickness (B) during biofilm growth, immobilization and remobilization of lead. The bars marked "air" mark the times when the biofilms were exposed to air, weeks 8–10, and weeks 16–18.

end of the 7th week in the biofilms grown on hematite and 60 g/L in the biofilms grown on quartz (Fig. 7B). The average biofilm densities decreased as a result of exposing the biofilms to the air, reaching, at the end of the 10th week, 60 g/L in the biofilms grown on hematite and 50 g/L in the biofilms grown on quartz. However, after resuming anaerobic conditions average biofilm densities slowly returned to the values they had at the end of the 7th week. Biofilm densities were similar during the anaerobic cycles of growth, at the ends of the 6th, 7th, 14th, and 15th weeks. At the end of the 18th week, after exposure to the air, biofilm densities decreased to values similar to those observed at the end of the 10th week: 60 g/L in the biofilms grown on hematite, and 55 g/L in the biofilms grown on quartz. This cycle, the decreasing and increasing of biofilm density, appears to be active every time the biofilms are exposed to air.

Fig. 7B shows that at the beginning of the process, biofilm thickness was increasing almost linearly, reaching at the end of the 8th week 250 μm in the biofilms grown on hematite and 220 μm in the biofilms grown on quartz. However, by the 10th week, biofilm thickness reached a maximum and was constant for the remaining time of operation. Introducing air into the reactors caused only negligible variations in biofilm thickness.

3.3. Iron in biofilms grown on hematite

Fig. 8 shows the amounts of iron found in the biofilms and in the bulk solution. The concentration of iron ions in the bulk solution was low, consistently near zero, and fluctuated within narrow limits. However, as time progressed, the amount of iron precipitated in the biofilms increased. In the 8-week-old biofilm, the amount of precipitated iron was estimated at 3 mg/cm^2, and exposing the biofilms to air increased that amount to 4 mg/cm^2 in two weeks. After the anaerobic growth conditions were resumed, the amount of iron in the biofilm did not change; it remained nearly constant until the biofilm was exposed to air again, which caused another increase in the amount of precipitated iron. Since the amount of precipitated iron increased rapidly after exposing biofilms to air, and the amount of dissolved iron in the bulk solution was very low during the anaerobic periods of operation, we conclude that

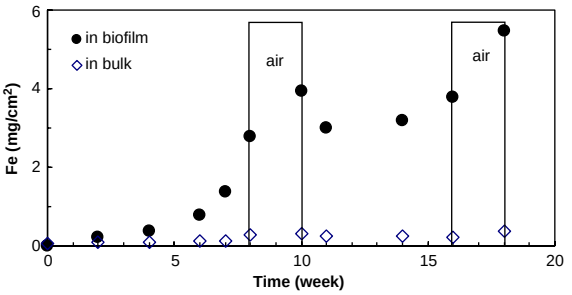

Fig. 8. Temporal changes in the amounts of iron immobilized in the biofilm, and dissolved in the bulk solution. Introducing air into the system increased the amount of iron released from the hematite. The data marked as "air" correspond to the time during which the reactor was continuously purged with filtered air and the growth medium was exposed to air.

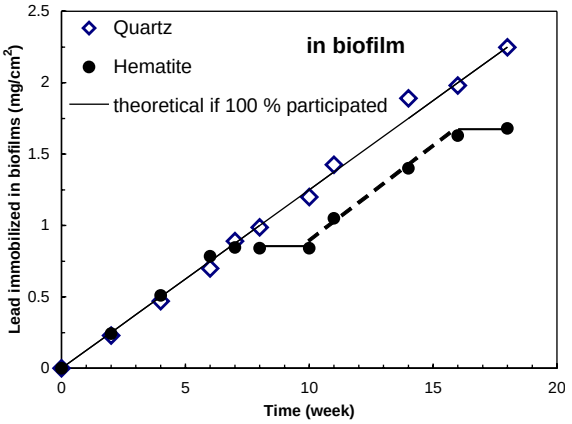

Fig. 9. The amounts of lead immobilized in the biofilms grown on hematite and on quartz. The continuous line shows a hypothetical result consistent with 100% removal of the lead introduced into the reactors for biofilms grown on quartz. When the biofilms were exposed to atmospheric oxygen, the lead immobilization on hematite slowed down. The dotted line shows the expected 100% removal of lead for biofilms grown on hematite. Note that due to significant detachment of the biofilm the lost lead caused a shift in the expected 100% immobilization line. As can be seen, all the lead in the biofilm grown on quartz was immobilized, while somewhat less lead was immobilized in the biofilm grown on hematite.

exposing the biofilms to the air increased the rate of iron release from the hematite.

3.4. Lead immobilization

The amounts of lead immobilized during biofilm growth on hematite and on quartz are shown in Fig. 9. The continuous line reflects the (hypothetical) response of the system if all lead were immobilized by the biofilms. The data show that lead was completely immobilized only in the biofilms grown on quartz; in the biofilm grown on hematite not all lead was immobilized. This difference can be related to the fact that in the biofilms grown on hematite both lead and iron were immobilized and, perhaps, the microbially generated hydrogen sulfide precipitated iron ions that were released near the substratum, the surface of hematite, at the location where most hydrogen sulfide was generated.

3.5. Biofilm–mineral interactions and the effects of biofilm structure

The hypothetical mechanism of biofilm–iron–lead interactions given in Fig. 1 appears to reflect the process of lead immobilization and remobilization quite accurately. According to this model, the microbially produced sulfide immobilizes both iron and lead in the biofilms grown on hematite. However, since the total amount of microbially generated sulfide is limited, iron and lead compete for the binding capacity of hydrogen sulfide, and the removal of lead is less efficient than it would be in biofilms grown on minerals that do not release iron. This conclusion needs to be reinforced by additional consideration. Judging from thermodynamics only, iron should not precipitate until all lead has precipitated. However, this expectation is based on thermodynamics only, and on the assumption that the reaction is occurring in a homogeneous solution. The biofilm matrix is not homogeneous, and mass transport resistance, and some effects related to reaction kinetics other than thermodynamics may be responsible for the observed deviations from expectations. In particular, we hypothesize that iron sulfide had precipitated because iron ions were generated at locations where lead ions were not accessible, near the surface of the mineral. Lead ions, being delivered from the surface, had to penetrate across the biofilm to reach the location where iron precipitated. In addition, most of the time lead concentration in the bulk solution was near zero, which sets the conditions favorably for precipitation iron ions released from hematite as FeS, according to Eq. (3). We tried to use XPS to quantify iron chemistry in the deposits; not very successfully however, because of high concentration of biomass accumulated on the surface.

The differences in biofilm chemistry are associated with the differences in biofilm structure, which may have been responsible for other observed effects. The biofilms grown on hematite and those grown on quartz had the same structure at the end of the 6th week, and showed identical capacity for lead immobilization (Fig. 9). However, after 16 weeks of operation, which included periodic exposure of the biofilms to oxygen, their structures were different: The biofilms grown on hematite had a higher porosity and a higher fractal dimension. The higher porosity may have allowed more oxygen to diffuse into the bottom layer of the biofilm when the biofilms were exposed to air. It is then conceivable that when the access of oxygen was permitted, the iron sulfides precipitated in the biofilm were reoxidized, and precipitated as iron oxides. That would explain why the biofilms grown on hematite had more rugged surfaces than the biofilms grown on quartz, as reflected by their higher fractal dimension.

Our results show that the maximum efficiency of metal immobilization in sulfate reducing biofilms can be accomplished when the minerals in the subsoil environment are redox-insensitive and do not release metals, e.g. quartz. Metals released from redox-sensitive minerals can precipitate with microbially generated H_2S and decrease the overall metal binding capacity of the system. The processes in which part of the hydrogen sulfide binds metals released from the minerals are possible because of kinetic limitations imposed by the

biofilm heterogeneity and the associated mass transport resistance, and may not necessarily be expected from thermodynamic calculations alone.

4. Conclusions

1. As expected, biofilms grown on hematite and on quartz were heterogeneous, composed of cell clusters and voids. However, the biofilms grown on hematite were more porous, and had higher fractal dimensions showing that they had more ragged surfaces than the biofilms grown on quartz.
2. The average H_2S concentration was higher in the biofilms grown on quartz than it was in the biofilms grown on hematite.
3. When the biofilms were exposed to the air, their porosity and fractal dimension increased and their density decreased.
4. During 18 weeks of operation, iron was releasing continuously from the hematite.
5. Lead precipitated more readily in biofilms grown on quartz.
6. Metals released from redox-sensitive minerals can precipitate with microbially generated H_2S and decrease the overall metal binding capacity of the contaminant metal.

Acknowledgements

This research work was supported by the US Department of Energy, Office of Science, Natural and Accelerated Bioremediation Research (NABIR) program by grants DE-FG03-98ER62630/A001 and DE-FG03-01ER63270 to Montana State University. The authors thank Dr. Judy D. Wall for donating *Desulfovibrio desulfuricans* (G20), Dr. Jim Amonette for analyzing the chemical structure of hematite chips, and Drs. Brent Peyton and Rajesh Sani for discussions and comments.

References

[1] Francis AJ, Dodge CJ. Remediation of soils and wastes contaminated with uranium and toxic metals. Environ Sci Technol 1998;32:3993–8.
[2] Ganesh R, Robinson KG, Reed GD, Sayler G. Reduction of hexavalent uranium from organic complexes by sulfate- and iron-reducing bacteria. Appl Environ Microbiol 1997;63:4385–91.
[3] Lovley DR, Widman P, Woodward J, Phillips EJP. Reduction of uranium by cytochrome c3 of *Desulfovibrio vulgaris*. Appl Environ Microbiol 1993;59:572–6.
[4] Panak P, Hard BC, Pietzsch K, Kutschke SR, Öske K, Selenska-Pobell S, Bernhard G, Nitsche H. Bacteria from uranium mining waste pile: interactions with U(VI). J Alloys Compounds 1998;271–273:262–6.
[5] Nemati M, Jenneman GE, Voordouw G. Mechanistic study of microbial control of hydrogen sulfide production in oil reservoirs. Biotechnol Bioeng 2001;74:424–34.
[6] Robert M, Berthelin J. Role of biological and biochemical factors in soil mineral weathering. In: Huang PM, Schnitzer M, editors. Interactions of soil minerals with natural organics and microbes. Madison, WI: Soil Science Society of America; 1986. p. 453–95.(Chapter 12) (Special Publication No. 17).
[7] Morel FMM, Hering JG. Principles and applications of aquatic chemistry. New York: Wiley; 1993. p. 245.
[8] Neal AL, Techkarnjanaruk S, Dohnalkova A, McCready D, Peyton BM, Geesey GG. Iron sulfides and sulfur species produced at hematite surfaces in the presence of sulfate-reducing bacteria. Geochim Cosmochim Acta, 2001;65:223–35.
[9] Nelson YM, Lo W, Lion LW, Shuler ML, Ghirorse WC. Lead distribution in a simulated aquatic environment: effects of bacterial biofilms and iron oxide. Water Res 1995;29:1934–44.
[10] Lee Gall J, Payne WJ, Chen L, Liu MY, Xavier AV. Localization and specificity of cytochromes and electron transfer proteins from sulfate reducing bacteria. Biochimie 1994;76:655–65.
[11] Thauer RK, Jungermann K, Decker K. Energy conservation in chemotrophiv anaerobic bacteria. Bacteriol Rev 1977;41:100–80.
[12] Stumm W, Morgan JJ. Aquatic chemistry. 3rd ed. New York: Wiley; 1996. p. 400.
[13] Jakobsen R, Postma D. Redox zoning, rates of sulfate reduction and interactions with Fe-reduction and methanogenesis in a shallow sandy aquifer, Romo, Denmark. Geochim Cosmochim Acta 1999;63: 137–51.
[14] Langmuir D. Aqueous environmental geochemistry. 1st ed. Englewood Cliffs, NJ: Prentice Hall, 1997. p. 120.
[15] Wall JD, Rapp-Giles BJ, Roussel M. Characterization of a small plasmid from *Desulfovibrio desulfuricans* and its use for shuttle vector construction. J Bacteriol 1993;175: 4121–8.
[16] Sani RK, Geesey G, Peyton BM. Assessment of lead toxicity to *Desulfovibrio desulfuricans* G20: influence of components of lactate C medium. Advances Environ Res 2001;5:269–76.
[17] Postgate JR. The sulfate reducing bacteria, 2nd ed.. Cambridge: Cambridge University Press; 1984.
[18] Beyenal H, Lewandowski Z. Mass transport dynamics, activity, and structure of sulfate reducing biofilms. AIChE 2001;47:1689–97.
[19] Jeroschewski P, Steuckart C, Kühl M. An amperometric microsensor for the determination of H_2S in aquatic environments. Anal Chem 1996;68:4351–7.
[20] Lewandowski Z, Beyenal H. Use of microsensors to study biofilms. In: Lens P, Moran AP, Mahony T, Stoodley P, O'Flaherty V, editors. Biofilms in medicine, industry and environmental biotechnology–Characteristics, analysis and control. London: IWA Publishing; 2003. p. 375–412.

[21] Lewandowski Z, Beyenal H. Limiting-current-type microelectrodes for quantifying mass transport dynamics in biofilms. In: Doyle RJ, editor. Microbial growth in biofilms: part B, methods enzymol, Vol. 337; 2001. p. 339–59.
[22] Kühl M, Steuckart C, Eickert G, Jeroschewski PA. H_2S microsensor for profiling biofilms and sediments: application in an acidic lake sediment. Aquat Microb Ecol 1998;15:201–9.
[23] Xia F, Beyenal H, Lewandowski Z. An electrochemical technique to measure local flow velocity in biofilms. Water Res 1998;32:3637–45.
[24] Yang X, Beyenal H, Harkin G, Lewandowski Z. Quantifying biofilm structure using image analysis. J Microbiol Methods 2000;39:109–19.
[25] Lewandowski Z, Webb D, Hamilton M, Harkin G. Quantifying Biofilm Structure. Water Sci Tech 1999; 39:71–6.
[26] Lewandowski Z. Notes on biofilm porosity. Water Res 2000;9:2620–4.
[27] Hermanowics SW, Schindler U, Wilderer P. Fractal structure of biofilm: new tools for investigation of morphology. Water Sci Tech 1995;32:99–105.